Applied Catalysis A: General 482 (2014) 344–351

Contents lists available at ScienceDirect

Applied Catalysis A: General

journal homepage: www.elsevier.com/locate/apcata

Dehydrogenation of ethylbenzene over zirconium-based perovskite-type catalysts of $AZrO_3$ (A: Ca, Sr, Ba)

Ryo Watanabe [a], Yoshinori Saito [b], Choji Fukuhara [a,*]

[a] Department of Applied Chemistry and Biochemical Engineering, Graduate school of Engineering, Shizuoka University, 3-5-1, Johoku, Naka-ku, Hamamatsu, Shizuoka, Japan
[b] Murata Manufacturing Co., Ltd., Nagaokakyo-shi, Japan

ARTICLE INFO

Article history:
Received 10 December 2013
Received in revised form 7 June 2014
Accepted 11 June 2014
Available online 19 June 2014

Keywords:
Dehydrogenation of ethylbenzene
Perovskite oxide catalyst
BaZrO3
Oxygen vacancy
ESR

ABSTRACT

The aim of this work was to investigate the catalytic performance of the $AZrO_3$ (A: Ca, Sr or Ba) catalysts for the dehydrogenation of ethylbenzene (EBDH) to produce styrene and to clarify an important factor for the high dehydrogenation activity. Among the $AZrO_3$ catalysts, only the $BaZrO_3$ (BZO) catalyst showed a significantly high activity for EBDH and the activity increased with time, while the $CaZrO_3$ and $SrZrO_3$ catalysts almost did not provide any activity at 823 K. Comparing the styrene yield over the BZO catalyst with that over the industrial potassium-promoted iron oxide (Fe–K) catalyst, the BZO catalyst showed a lower styrene yield than the Fe–K catalyst at the initial stage of the reaction. However, after 40 min of EBDH, the BZO catalyst exhibited a higher styrene yield than the Fe–K catalyst. Based on an ESR measurement, a sharp signal at $g = 2.004$, which was identified as an unpaired electron trapped in oxygen vacancies, was detected in the BZO catalyst after dehydrogenation. The number of oxygen vacancies increased with change in the dehydrogenation activity. In addition, the BZO catalyst with a pretreatment by H_2 reduction presented a high activity without an induction period. Comparing the profiles of the temperature desorption of ethylbenzene (EB) over the prereduced catalyst to that of the untreated BZO catalyst, a chemisorbed species of EB was detected over the prereduced BZO catalyst, although a physisorbed species was present on the surface of the untreated catalyst. Hence, the production of oxygen vacancies opened the adsorption channel of EB and created the reactive site, which produced a high EBDH activity.

1. Introduction

Zirconium (Zr)-based materials, such as a yttria-stabilized ZrO_2 and a $Ce_xZr_{1-x}O_2$, have been applied to a variety of applications in ceramics, solid oxide fuel cells, oxygen sensors, and catalysts [1–8]. The success of Zr-based materials for widespread applications is mainly derived from its oxygen mobility coupled with the redox ability of these oxides. Despite its diverse applications, the investigation of the catalysis of the Zr-based perovskite materials has not been performed until recently. Perovskite-type mixed oxides (general formula ABO_3, A is a rare-earth or an alkali-earth element and B is typically a transition metal) have a high lattice oxygen mobility in comparison to common transition metal oxides, and in addition, the redox ability could be controlled by changing the incorporated element [9–12]. In addition, they have a much better thermal stability than transition metal oxides and their catalytic activities are sometimes competitive with supported noble metal catalysts [13].

In a preliminary study, the catalytic activity for the dehydrogenation of ethylbenzene (EBDH) to produce styrene (Eq. 1) has been examined over Mn- and Fe-based perovskite-type oxides [14].

$$C_8H_{10} \rightarrow C_8H_8 + H_2 \quad (1)$$

As a result, a $La_{0.8}Ba_{0.2}Fe_{0.4}Mn_{0.6}O_{3-\delta}$ (denoted as LBFMO) catalyst had a high performance and revealed an activity superior to the industrial Fe–K catalyst at the low temperature of 813 K. In addition, the catalytic activity and stability were found to depend on the redox characteristics of the perovskite material [15,16].

The La element, which was contained in the LBFMO catalyst, is an expensive rare-earth metal and unevenly distributed around the world. The price of such a rare earth metal element (denoted as REE) has gradually increased since 1995. By 2010, the REE was traded at a very high price; La oxide was 6.2–6.5 US$/kg, Ce oxide was 4.7–5.2 US$/kg, Pr oxide was 30–30.5 US$/kg and Nd oxide

* Corresponding author. Tel.: +81 53 478 1171; fax: +81 53 478 1172.
E-mail address: tcfukuh@ipc.shizuoka.ac.jp (C. Fukuhara).

http://dx.doi.org/10.1016/j.apcata.2014.06.012
0926-860X/

was 30.5–31 US$/kg [17]. Therefore, the lanthanoid element as the A-site cation cannot be included in the catalyst for industrial applications due to its cost. However, the price of a divalent metal, such as Ba, was low compared to the rare earth metal. Barite, which is a raw material of Ba, is trading at 30 US$ per ton. The advantage is not only its availability, but also the adequate catalytic performance of perovskite catalysts containing a divalent cation. The incorporation of an alkaline earth metal, such as Ca^{2+}, Sr^{2+} and Ba^{2+}, into the A-site of the perovskite structure would generate electron holes and oxygen vacancies as the charge compensation. Such an incorporation of the divalent cation could induce a high oxygen mobility derived from the mixed conduction by an electron and oxygen ion [18–20]. Additionally, the incorporation of elements with a large ionic radii, such as Ba, into the A-site of the perovskite structure produces a high free volume in the lattice, which decreases the activation energy of the oxygen ion migration [21,22]. These effects promoted the releasing rate of the lattice oxygen, thus expecting a high performance for the EBDH.

As already mentioned, the A-site substitution by the divalent cation could provide a high redox flexibility of the perovskite-type oxide. Thus in the present study, the catalytic performances of the Zr-based perovskite catalysts containing a divalent cation, such as Ca, Sr and Ba, were investigated, and compared to that over the industrial potassium-promoted iron oxide catalyst (Nissan Girdler Catalyst; G-84C). In addition, an important factor for the dehydrogenation activity over the $BaZrO_3$ perovskite catalyst was investigated in terms of the structural state measured by X-ray diffraction, the catalyst morphology observed by field emission scanning electron microscopy and its oxidation state measured by electron spin resonance.

2. Experimental

2.1. Catalyst preparation

The zirconium-based perovskite oxides of $AZrO_3$ (A: Ca, Sr, Ba) were prepared by the solid state reactions of ZrO_2 and an alkali carbonate. These powders were thoroughly mixed in an agitate mortar, pelletized and then calcined at 1373 K for 12 h. The industrial potassium-promoted iron oxide (G-84C, made by Nissan Girdler K.K.; composition = 77 wt%-Fe_2O_3, 10 wt%-K_2O, 5.0 wt%-Ce_2O_3, 2.5 wt%-MoO_3, 2.2 wt%-CaO, 2.2 wt%-MgO, and less than 0.1 wt%-of Cr_2O_3) catalyst was used as the reference catalyst.

2.2. Activity test

The catalytic activity, selectivity and stability of the prepared catalyst for the dehydrogenation of ethylbenzene (EBDH) were examined using a conventional fixed bed reactor. The reactor used in this study consisted of a quartz tube (10-mm o.d.) containing a catalyst bed, which was fixed by quartz wool. A type-K thermocouple for controlling the temperature was positioned outside the quartz tube. The reactions were conducted at 823 K under atmospheric pressure. The weight hourly space velocity (WHSV, EB based) was 1.2–24 h^{-1} and the EB supplied to the catalyst bed was diluted by helium (P_{EB}: 6.3 kPa). The catalyst weight was 0.005–1.0 g. Liquid products such as EB, benzene, toluene, and styrene were analyzed using an off-line thermal conductivity detection (TCD) gas chromatograph (GC-8A; Shimadzu Co. Ltd., Japan). The conversion (Eq. 2), styrene yield (Eq. 3) and styrene selectivity (Eq. 4) were determined using the following equations.

$$\text{EB conversion} = \frac{[\text{Sty}] + [\text{Bz}] + [\text{Tol}]}{[\text{EB}] + [\text{Sty}] + [\text{Bz}] + [\text{Tol}]} \times 100 \quad (2)$$

$$\text{Styrne yield} = \frac{[\text{Sty}]}{[\text{Sty}] + [\text{Bz}] + [\text{Tol}]} \times \text{EB conversion} \quad (3)$$

$$\text{Styrne selectivity} = \frac{[\text{Sty}]}{[\text{Sty}] + [\text{Bz}] + [\text{Tol}]} \times 100 \quad (4)$$

[EB], [Sty], [Bz], and [Tol] denote the concentration of EB, styrene, benzene and toluene in the effluent gas, respectively. The carbon balances in this study were over 95% for all the experimentally obtained results.

2.3. Characterization of the catalyst

The crystalline structure of the prepared catalyst was ascertained using an X-ray powder diffraction with Cu*K*α radiation (λ = 1.54 Å, Rint-2000; Rigaku Co. Ltd., Japan). The specific surface area of the zirconium-based perovskite oxide was analyzed by the N_2 absorption method (Model 4200; Nikkiso Co. Ltd., Japan). The sample was outgassed at 423 K for 30 min before absorbing N_2.

X-ray photoelectron spectroscopy (XPS, Quantum2000; Physical Electronics Co. Ltd., USA) measurements were performed using non-monochromatic Al*K*α radiation. The pass energy of the analyzer was 23.5 eV. The binding energy of C_{1s} at 284.7 eV was used for calibration.

In order to study the morphology of the BZO catalyst, a field emission scanning electron microscopy (FE-SEM) measurement was performed using a SU8040 (Hitachi High-Technologies Corporation, Japan). The ESR spectra were obtained by an EMX spectrometer (Bruker BioSpin Corp., USA) at the field modulation of 100 kHz, an amplitude modulation of 0.8 mT and a microwave power of 0.02 mW. The measurement was performed at room temperature and in ambient air without vacuum-pumping. A sharp signal at $g = 2.004$, which was identified as one electron trapped in V_{ox}, was detected, and the number of V_{ox} was calculated from the sharp signal using the following equation.

$$N_{\text{el,sample}} = N_{\text{el,standard}} \times \frac{S_{\text{sample}}}{S_{\text{standard}}} \quad (5)$$

$$N_{\text{vox}} = N_{\text{el,sample}} \quad (6)$$

$N_{\text{el, sample}}$ and $N_{\text{el, standard}}$ are the number of electron spins in the catalyst and in the standard sample of $CuSO_4{\cdot}5H_2O$, respectively. The number of electron spins which is included in the standard sample of 1 g is 2.41×10^{21}. S_{sample} and S_{standard} are the signal areas of the catalyst and the standard sample, respectively. N_{Vox} is the number of oxygen vacancies with an unpaired electron in the catalyst.

Temperature-programmed desorption (TPD) was performed in order to investigate the surface active site, and adsorption and desorption properties with increasing temperature. Before the TPD measurement, EB (4.6 kPa) was supplied to the catalyst (0.50 g) at 323 K for 30 min as a pretreatment. After the EB adsorption on the catalyst, EB in gas phase was completely purged by helium (He) for 2 h. The catalyst was then heated in He (100 ml min^{-1}) at 10 K min^{-1} from 323 to 1073 K. The effluent gas was monitored by an on-line Omnistar GSD301 quadrupole mass spectrometer (Pfeiffer Vacuum, Germany). The parent peak of EB was scanned by the mass spectrometer: m/z; 91 (EB).

3. Results and discussion

3.1. Characterization of the $AZrO_3$ (A: Ca, Sr, Ba) catalysts

Fig. 1 shows the structural states of the $AZrO_3$ (A: Ca, Sr, Ba) and ZrO_2 catalysts measured by XRD. Hereafter, the $CaZrO_3$ catalyst was abbreviated as CZO, the $SrZrO_3$ catalyst as SZO, and the $BaZrO_3$ as BZO. The SZO and BZO catalysts showed the typical

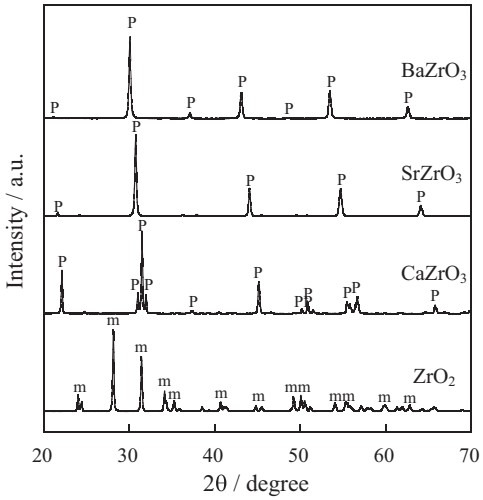

Fig. 1. XRD patterns of $AZrO_3$ (A: Ca, Sr, Ba) and ZrO_2 materials. The symbol "P" was for perovskite; and "m" was for monoclinic.

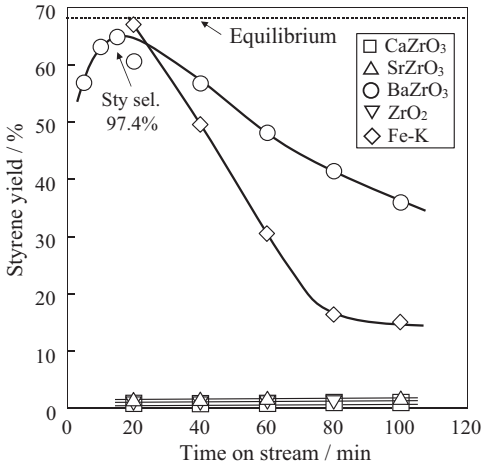

Fig. 2. Styrene yield over $AZrO_3$ (A: Ca, Sr, Ba), ZrO_2 and potassium-promoted iron oxide catalysts for EBDH under the following condition: the feed rate of EB was 1.2 g h^{-1}; the catalyst weight was 1.0 g; and the reaction temperature was 823 K.

perovskite structure [23]. The CZO catalyst also showed a perovskite structure, although the XRD pattern of the CZO was different from those of the SZO and BZO catalysts [24]. The SZO and BZO have an ideal perovskite structure, while the CZO structure is composed of a distorted ZrO_6 octahedra. Due to this distortion, the coordination of the Ca^{2+} ion is reduced from 12 in ideal perovskite to 8 in the CZO. The difference in the XRD pattern might come from such a distortion of the perovskite material, while the ZrO_2 has only a monoclinic phase in the material. Table 1 presents the specific surface area of the perovskite oxides and ZrO_2. The specific surface area increased with an increase in the atomic radius of the A-site cation in the zirconium-based perovskite-type oxides.

3.2. Dehydrogenation performance over the $AZrO_3$ (A: Ca, Sr, Ba) catalysts

The EBDH properties over the AZO (A: Ca, Sr, Ba) perovskite-type oxide catalysts and ZrO_2 were investigated for clarifying their ability to produce styrene at the low temperature of 823 K. The feed rate of EB was 1.2 g h^{-1}, and the catalyst weight was 1.0 g. Fig. 2 shows the styrene yield with time over these catalysts. The Fe–K industrial catalyst (G-84C, made by Nissan Girdler K.K.) was utilized as the reference. As shown in Fig. 2, the CZO, SZO and ZrO_2 catalysts did not show any dehydrogenation activity at 823 K. On the other hand, the BZO catalyst showed an induction period of about 15 min, and the activity passed through a maximum with time, followed by a slow deactivation. The maximum styrene yield of 64.9% with a 97.4% styrene selectivity was obtained, which was relatively close to the equilibrium value. The styrene yield then decreased to 36.0% at 100 min of reaction. The Fe–K catalyst represented the high initial styrene yield of 67.0% and styrene selectivity of 98.7% at 20 min. The styrene yield then decreased to 15.0% at 100 min. Comparing the styrene yield over the BZO catalyst with that over the industrial Fe–K catalyst, the BZO catalyst had a slightly lower dehydrogenation activity at 20 min. However, the BZO catalyst showed a higher styrene yield than the Fe–K catalyst after 40 min of EBDH.

In order to examine the effect of the reaction temperature on the dehydrogenation performance, activity tests over the AZO (A: Ca, Sr or Ba) and ZrO_2 catalysts were performed within the temperature range of 823–923 K. The feed rate of EB was 1.2 g h^{-1}, and the catalyst weight was 0.05 g for the BZO, 0.2–0.4 g for the SZO, 0.1–0.8 g for the CZO and 0.8 g for ZrO_2 catalysts, respectively. The styrene yield versus time is shown in Fig. 3. In addition, Fig. 4(a) denotes the maximum formation rate of styrene over these catalysts at each reaction temperature, which was obtained from Fig. 3. From Fig. 3(a) and (b), an induction period was observed over the CZO and SZO catalysts. The induction period became shorter at the higher temperatures. The BZO catalyst showed a high dehydrogenation activity at a lower reaction temperature than the other catalysts, while the ZrO_2 catalyst showed a significantly low dehydrogenation activity and did not have an induction period. Fig. 4(b) shows the styrene selectivity over the AZO (A: Ca, Sr, Ba) catalysts and the ZrO_2 catalyst at each reaction temperature. Among these catalysts, the BZO catalyst showed the highest selectivity to styrene. The CZO and SZO catalysts also had a high selectivity to styrene, but the ZrO_2 catalyst showed a relatively low selectivity. The reason for the induction period and the higher dehydrogenation activity over the BZO catalyst is considered in Sections 3.3–3.6.

Table 1
Specific surface area of $AZrO_3$ (A: Ca, Sr, Ba) and ZrO_2 catalysts.

Catalyst	Specific surface area (m^2 g-cat^{-1})
$CaZrO_3$	2.1
$SrZrO_3$	4.7
$BaZrO_3$	10.0
ZrO_2	0.2

3.3. Bulk property of the BZO catalyst

For investigating the relation between the gradual increase in the dehydrogenation activity and the structural change in the BZO catalyst, XRD measurements of the used BZO catalysts were conducted. The used catalyst was defined as the BZO catalyst after EBDH, and the styrene yield over the used catalyst is shown in parenthesis. Four kinds of used BZO catalysts (3.7), (35.5), (55.4) and (57.3 → 47.2) were characterized. The used catalyst (57.3 → 47.2) means the degraded value (47.2% styrene yield) after the maximum yield (57.3%). These catalysts are the same lot, which was prepared by the same method. Each catalyst had a different time courses of the EBDH reaction. For example of the BZO (3.7), the reaction was purposely stopped at the time when the BZO catalyst showed the styrene yield of 3.7%. Other catalysts was obtained in the same way. Fig. 5 shows the XRD patterns of the used BZO catalysts. A structural change and a peak shift were not observed in these XRD patterns. The lattice constant of all the used catalysts was 4.193 Å. The bulk property of the catalyst was not affected by the reaction gas. The

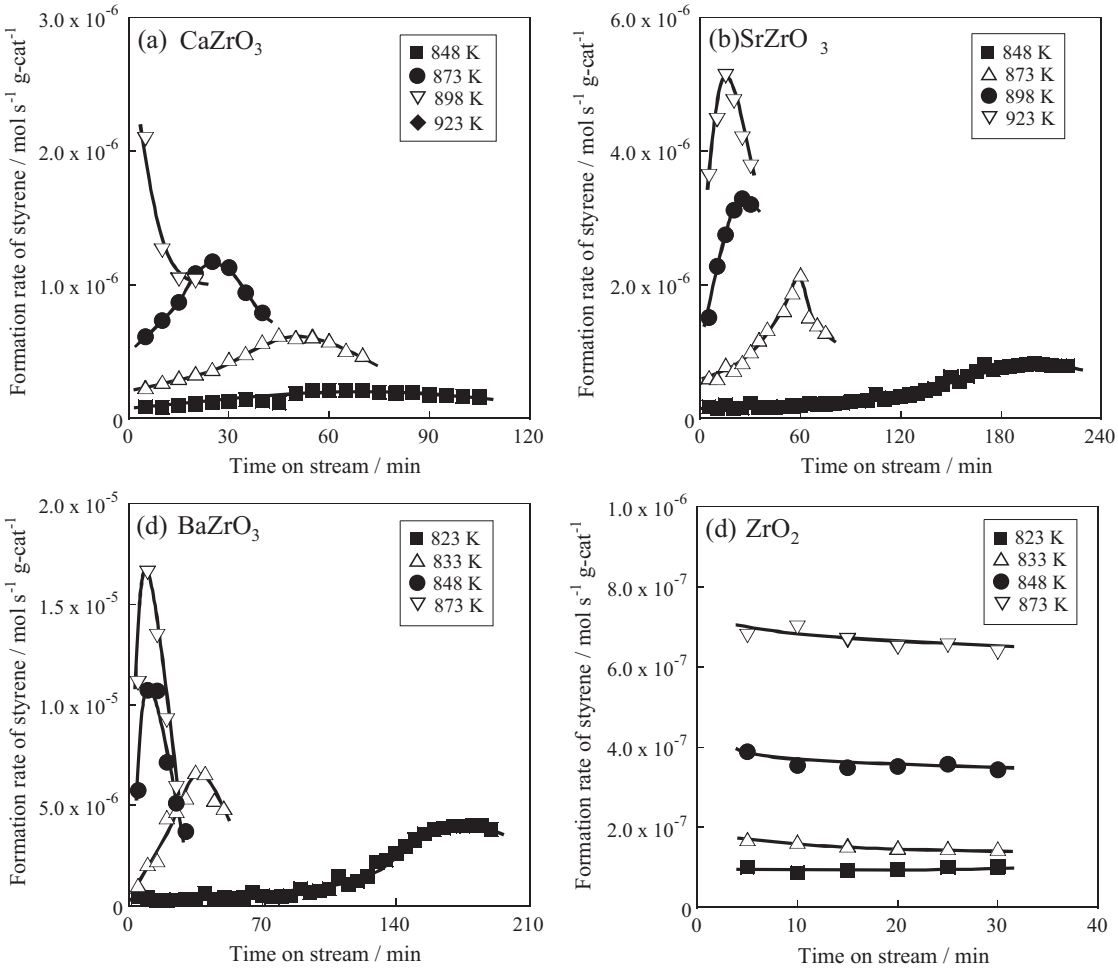

Fig. 3. Styrene yield versus time over (a) $CaZrO_3$, (b) $SrZrO_3$, (c) $BaZrO_3$ and (d) ZrO_2 catalysts under the following condition: the feed rate of EB was 1.2 g h^{-1}; the catalyst weight was 0.05 g for the BZO, 0.2–0.4 g for the SZO, 0.1–0.8 g for the CZO and 0.8 g for ZrO_2 catalysts; and the reaction temperature was from 823 to 923 K.

morphology of the BZO catalyst would not change with time. For confirming the shape of the catalyst, FE-SEM images of the used catalysts were obtained as shown in Fig. 6. From Fig. 6(b) and (d), the cubic BZO crystal was observed over the BZO (3.7) and BZO (57.3 → 47.2) catalysts. The crystal diameter of these catalysts was almost the same of about 50 nm. Comparing to the morphology and the cubic diameter of both catalysts, these structural property did not change, in spite of a different in the catalytic activity. Hence, we postulated that the induction period was not related to the bulk structural property and the morphology of the BZO catalyst.

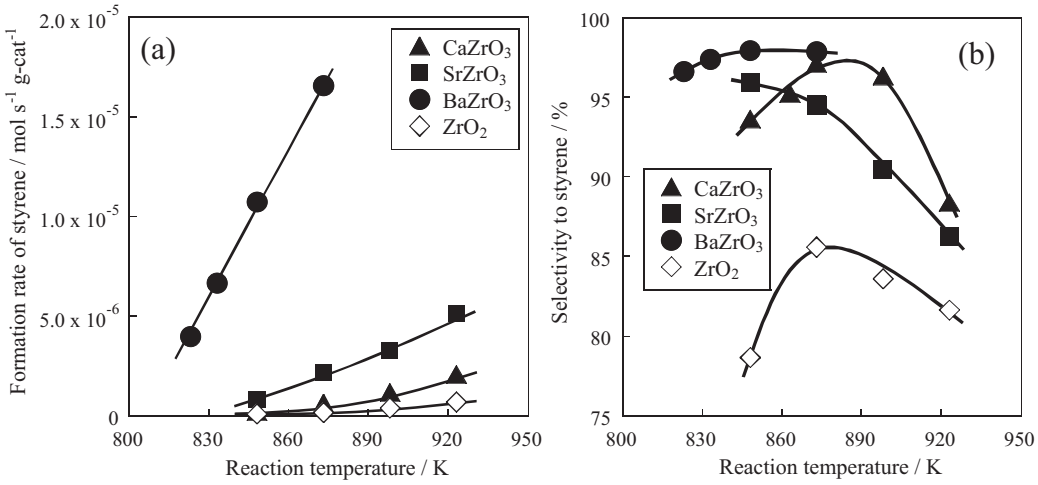

Fig. 4. Effect of reaction temperature on (a) maximum formation rate of styrene and (b) styrene selectivity over $AZrO_3$ (A: Ca, Sr, Ba) catalyst for EBDH.

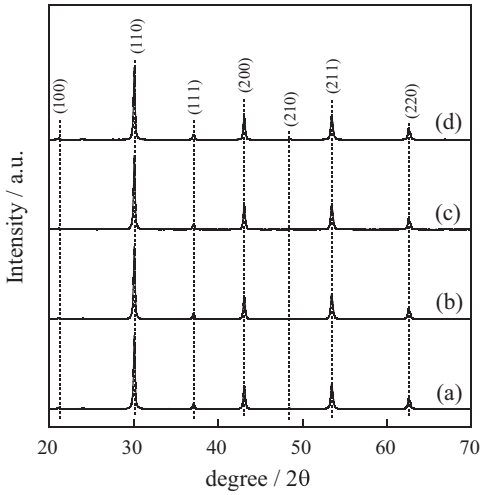

Fig. 5. XRD patterns of (a) BZO (3.7), (b) BZO (35.5), (c) BZO (55.4) and (d) BZO (57.3 → 47.2) catalysts.

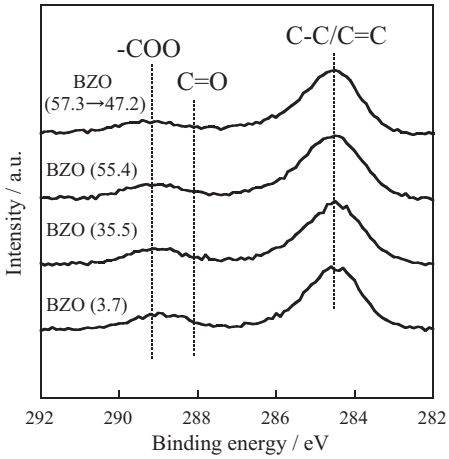

Fig. 7. C_{1s} XPS spectra of the used BZO catalyst.

3.4. Surface property for the BZO catalyst

Osswald et al. mentioned that unsaturated ketone-/diketone-type carbonyl groups (C=O) have a substantial electron density around the oxygen atom, and thus can serve as a Lewis bases to activate saturated hydrocarbons [25]. For clarifying whether or not carbonyl groups were confirmed on the used catalysts, X-ray photoelectron spectroscopy (XPS) analysis of the used catalysts was performed. The peak intensity of carbonyl group (C=O) would increase if the carbonyl group were accumulated on the catalyst with time on stream. The XPS spectra of C_{1s} for these catalysts are shown in Fig. 7. The peaks at 284.4, 288.1 and 290.2 eV were assigned to C–C/C=C, C=O and O=C–O, respectively [26]. Comparing to the peaks of the carbonyl group (C=O) at 288.1 eV over the four used BZO (3.7), (35.5), (55.4) and (57.3 → 47.2) catalysts, the peak intensities were almost the same. Namely, the amount of the carbonyl group might not increase on the catalyst with time courses. Hence, the carbonyl group on the used BZO would not affect the dehydrogenation activity of the BZO catalyst.

To obtain information on the reduced state of the BZO catalyst, ESR spectra for the used catalysts were recorded at room temperature as shown in Fig. 8. The used BZO catalyst gave the ESR signal at $g = 2.004$, whose g-value corresponded to oxygen vacancies in the catalyst [27]. The intensity of the signal at $g = 2.004$ was found to increase with an increase in the styrene yield. Therefore, the number of oxygen vacancies was calculated for relating the activity and oxygen vacancy in the catalyst.

Table 2 shows the area of each peak and the number of oxygen vacancies (denoted as N_{vox}). These areas of the signal at $g = 2.004$ increased as follows: 9.2×10^6 for the BZO (3.7%), 9.8×10^6 for the BZO (35.5%), and 13.5×10^6 for the BZO (55.4%). Comparing to the calculated N_{vox} from these areas, the N_{vox} increased with the increase in the styrene yield: 4.8×10^{18} mol-cat^{-1} for the BZO (3.7%), 5.2×10^{18} mol-cat^{-1} for the BZO (35.5%), and 7.5×10^{18} mol-cat^{-1} for the BZO (55.4%). There was a tendency that the number of oxygen vacancies increased with the increase in the catalytic activity. The increase in the number of oxygen vacancies suggested that

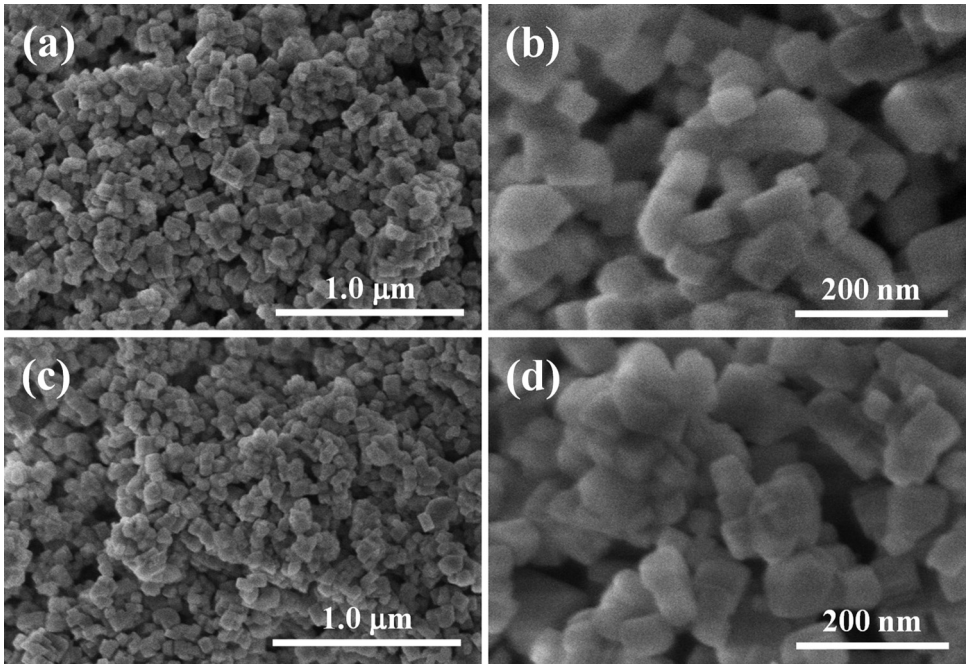

Fig. 6. FE-SEM images of (a), (b) BZO (3.7) catalyst and (c), (d) BZO (57.3 → 47.2) catalyst. Magnification: (a), (c) ×50,000 and (b), (d) ×200,000.

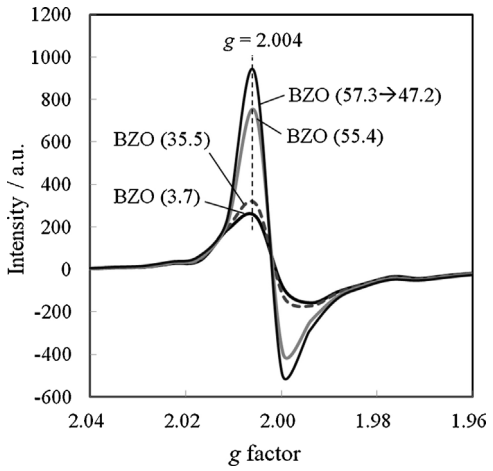

Fig. 8. ESR spectra of the used BZO catalyst.

Table 2
The number of oxygen vacancies (N_{Vox}) in the used BZO catalyst.

Catalyst[a]	Area ($\times 10^6$)	N_{Vox} ($\times 10^{18}$ mol-cat^{-1})
BZO (3.7)	9.2	4.8
BZO (35.5)	9.8	5.2
BZO (55.4)	13.5	7.5
BZO (57.3 → 47.2)	15.8	8.5

[a] The value in parenthesis is the styrene yield.

the BZO catalyst was gradually reduced during the dehydrogenation reaction. Hence, the reduced state of the BZO catalyst might have an impact on the dehydrogenation activity. So far, there have been some reports about the effect of the Fe component reduction in the Fe–K catalyst on its EBDH performance [28,29]. It was mentioned that a deactivation occurred by reduction of the hematite catalyst to the magnetite-type. Zhu et al. also insisted that the partial reduction of the Fe^{3+}-containing iron oxide phases caused the fast initial deactivation [30]. On the other hand, Weiss et al. investigated the role of the iron oxide stoichiometry and the defect-site on the catalytic activity [31]. They concluded that the styrene formation rate increased with the increasing defect-site concentration, and the defect-site was the active site for the EB dehydrogenation over Fe_2O_3. In this study, the reduced state of the catalyst may contribute to the enhancement of the dehydrogenation activity. These results were considered to be the important results, and should be further verified in the next section.

3.5. *Effect of reduced state in the BZO catalyst on the dehydrogenation performance*

The EBDH performance of the BZO catalyst, which was prereduced and/or prereduced followed by oxidation, was investigated to clarify the effect of the reduced state of the BZO catalyst. Fig. 9(a) shows the styrene yield with time over the BZO catalysts without pretreatment, with prereduction by 10 vol%-H_2 at 798 or 823 K, with prereduction by 100 vol%-H_2 at 923 K and with prereduction

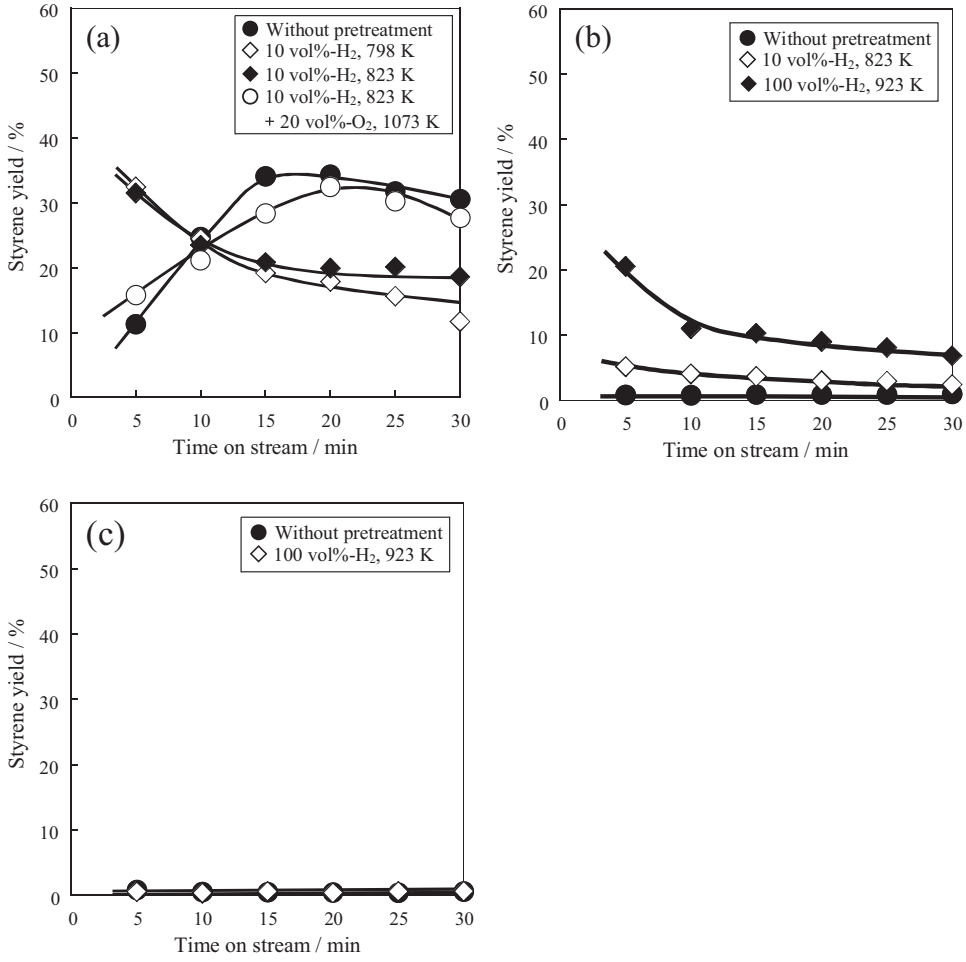

Fig. 9. Effect of prereduction by H_2 on the catalytic performance of (a) BZO, (b) SZO and (c) ZrO_2 at 823 K. The feed rate of EB was 1.2 g h^{-1} and the catalyst weight was 0.2 g for BZO, 1.0 g for SZO and ZrO_2.

by 10 vol%-H_2 at 823 K followed by oxidation by 20 vol%-O_2 at 1073 K. The feed rate of EB was 1.2 g h^{-1}, and the catalyst weight was 0.2 g. As clearly seen from Fig. 9(a), the BZO catalyst with pretreatment by H_2 reduction represented a high activity without the induction period. On the other hand, the induction period was observed again over the BZO catalyst with prereduction by H_2 at 823 K followed by oxidation with O_2 at 1073 K. These phenomena were considered to be based on the following Eqs. (7) and (8), where $O^{2-}{}_{lat}$ and V_{ox} denote a lattice oxygen and an oxygen vacancy in the catalyst, respectively.

$$H_2 + O^{2-}{}_{lat} \rightarrow H_2O + V_{ox} + 2e^- \quad (7)$$

$$O_2 + V_{ox} + 4e^- \rightarrow 2O^{2-}{}_{lat} \quad (8)$$

When the BZO catalyst was reduced by H_2, the oxygen vacancy was created based on Eq. (7). Thus, the BZO catalyst showed a high activity during the initial stage of the dehydrogenation. By reduction followed by oxidation, the lattice oxygen was replenished based on Eq. (8). Hence, the induction behavior was again confirmed over the BZO catalyst. Fig. 9(b) shows the effect of prereduction at 823 K by 10 vol%-H_2 or 923 K by 100 vol%-H_2 on the dehydrogenation performance over the SZO catalyst. The SZO catalyst without pretreatment did not show a dehydrogenation activity at 823 K. When the reduction was performed over the SZO catalyst, the representation of the dehydrogenation activity was confirmed. Such a result was considered to be derived from the progression of the reduction due to Eq. (7). A further increase in the H_2 concentration and reduction temperature from 10 vol%-H_2 at 823 K to 100 vol%-H_2 at 923 K produced a higher activity. Fig. 9(c) shows the catalytic behavior over the ZrO_2 catalyst with or without reduction. Unlike the BZO and SZO catalysts, the ZrO_2 catalyst did not produce any dehydrogenation activity even after prereduction by 100 vol%-H_2 at 923 K. The ZrO_2 catalyst might not be reduced even under the reductive atmosphere.

The BZO and SZO catalysts showed a dehydrogenation activity by reduction of the catalysts, while the ZrO_2 did not reveal any activity even if the prereduction was performed. By inserting Zr in the perovskite-type structure, a reducibility of the catalyst might be enhanced. Especially, the incorporation of Ba as the A-site cation would be the most effective for lowering the reduction temperature. The incorporation of Ba with a large ionic radii in the A-site of the perovskite structure produces a large free volume in the lattice, which provides a high mobility for the lattice oxygen. Such an effect could create oxygen vacancies in the BZO structure under a mild reducing atmosphere.

3.6. *Effect of reducing state of the BZO catalyst on EB adsorption/desorption properties*

In order to examine the effect of the reducing state of the catalyst on EB adsorption/desorption properties, a temperature-programmed desorption (TPD) was performed. Fig. 10 shows the EB-TPD profiles of the BZO catalyst with or without prereduction by H_2 at 823 K. From the TPD profile of the bare BZO catalyst, the profile of EB (m/z = 91) desorption showed one sharp signal in region (I). The signal in region (II) was almost not observed. The region (I) signal below 423 K came from the physical adsorption of the EB species, whereas the region (II) signal above 423 K was derived from the chemical adsorption of the EB species. The desorption profile indicated that the EB species with a weak interaction was present on the BZO catalyst without prereduction. For the BZO catalyst with prereduction, the some signals were observed in regions (I) and (II). As clearly be seen from the profile, the signal intensity for region (I) was significantly lower than that for region (II). In other words, the catalyst surface was covered by the EB species with a strong interaction on the catalyst surface. The differences in the TPD profiles of

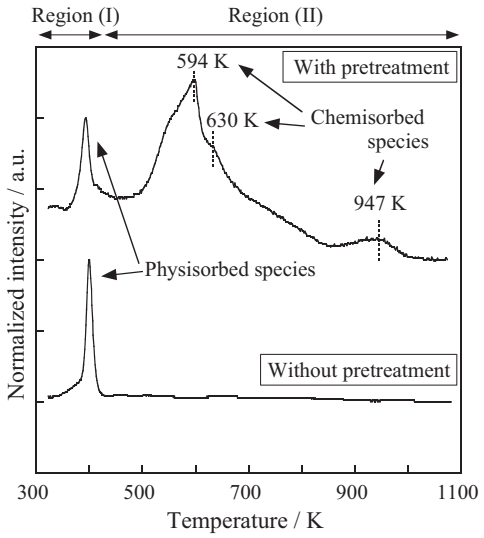

Fig. 10. Profiles of temperature programmed desorption of EB over the BZO catalyst with and without prereduction by H_2.

the BZO catalyst with or without prereduction could be explained by the different adsorption sites on the catalyst. Since the outermost surface layer of the as-made BZO catalyst consisted of lattice oxygen, no chemical interaction of EB occurred on the oxygen terminated BZO surface. Joseph et al. investigated the adsorption of EB on a well-ordered epitaxial iron oxide model catalyst by near-edge X-ray absorption fine structure spectroscopy [32]. The soft basic aromatic molecules of EB were chemisorbed on the acidic iron sites of the iron oxide catalyst surfaces. Therefore, in this study, the almost absence of chemisorbed species on the bare BZO catalyst might come from a repulsive electrostatic interaction between the surface lattice oxygen and the π orbital in EB. As for the BZO catalyst with prereduction, the surface lattice oxygen was removed by H_2, and the Zr cation as the acidic site was then exposed on the catalyst surface. Namely, the production of the oxygen vacancy opened the EB adsorption channel, and chemisorption species were observed as shown by the higher desorption temperature. Therefore, the increase in the oxygen vacancy created the reactive site for EBDH, which produced a high activity over the BZO catalyst.

4. Conclusions

The BZO catalyst produced a high activity for EBDH at the low temperature of 823 K, while the CZO, SZO and ZrO_2 catalysts did not show a EBDH activity. The reason for the high activity over the BZO catalyst was derived from the production of oxygen vacancies during the EBDH reaction, as confirmed by ESR measurements and some activity tests. Comparing the EB-TPD property of the as-made and the reduced BZO catalysts, the physisorbed species was mainly present on the as-made catalyst, whereas the chemisorbed species was on the reduced catalyst. The key point of the high activity over the Zr-based perovskite-type catalyst was the reduced state under the stated reaction conditions.

References

[1] J.-H. Lee, H. Moon, H.-W. Lee, J. Kim, J.-D. Kim, K.-H. Yoon, Solid State Ionics 148 (2002) 15–26.
[2] E.S. Hech, G.K. Gupta, H. Zhu, A.M. Dean, R.J. Kee, L. Maier, O. Deutschmann, Appl. Catal. A: Gen. 295 (2005) 40–51.
[3] H. Koide, Y. Someya, T. Yoshida, T. Maruyama, Solid State Ionics 132 (2000) 253–260.
[4] S. Yu, Q. Wu, M. Tabib-Azar, C.-C. Liu, Sens. Actuators B 85 (2002) 212–218.
[5] N. Rajabbeigi, B. Elyassi, A. Khodadadi, S.S. Mohajerzadeh, M. Sahimi, Sens. Actuators B 100 (2004) 139–142.

[6] S.M. de Lima, I.O. da Cruz, G. Jacobs, B.H. Davis, L.V. Mattos, F.B. Noronha, J. Catal. 257 (2008) 356–368.
[7] S.M. de Lima, A.M. Silva, I.O. da Cruz, G. Jacobs, B.H. Davis, L.V. Mattos, F.B. Noronha, Catal. Today 138 (2008) 162–168.
[8] P.P. Silva, F.A. Silva, H.P. Souza, A.G. Lobo, L.V. Mattos, F.B. Noronha, C.E. Hori, Catal. Today 101 (2005) 31–37.
[9] R.J.H. Voorhoeve, J.P. Remeika, L.E. Trimble, Ann. N. Y. Acad. Sci. 272 (1976) 3–21.
[10] T. Nitadori, T. Ichiki, M. Misono, Bull. Chem. Soc. Jpn. 61 (1988) 621–626.
[11] Y. Teraoka, H.M. Zhang, K. Okamoto, N. Yamazoe, Mater. Res. Bull. 23 (1988) 51–58.
[12] H.M. Zhang, Y. Shimizu, Y. Teraoka, N. Miura, N. Yamazoe, J. Catal. 121 (1990) 432–440.
[13] M.A. Peña, J.L.G. Fierro, Chem. Rev. 101 (2001) 1981–2017.
[14] R. Watanabe, Y. Sekine, M. Matsukata, E. Kikuchi, Catal. Lett. 131 (2009) 54–58.
[15] R. Watanabe, Y. Sekine, J. Kojima, M. Matsukata, E. Kikuchi, Appl. Catal. A: Gen. 398 (2011) 66–72.
[16] R. Watanabe, K. Mukawa, J. Kojima, E. Kikuchi, Y. Sekine, Appl. Catal. A: Gen. 462–463 (2013) 168–177.
[17] http://www.bgs.ac.uk/mineralsuk/home.html
[18] S. Li, W. Jin, P. Huang, N. Xu, J. Shi, Ind. Eng. Chem. Res. 38 (1999) 2963–2972.
[19] Y. Teraoka, T. Nobunaga, N. Yamazoe, Chem. Lett. 88 (1988) 503–506.
[20] J.W. Stevenson, T.R. Armstrong, R.D. Carmeim, L.R. Pederson, L.R. Weber, J. Electrochem. Soc. 143 (1996) 2722–2729.
[21] R.L. Cook, A.F. Sammells, Solid Sate Ionics 45 (1991) 311–321.
[22] J. Hu, H. Hao, C. Chen, D. Yang, X. Hua, J. Membr. Sci. 280 (2006) 809–814.
[23] J. Huang, L. Zhou, Z. Wang, Y. Lan, Z. Tong, F. Gong, J. Sun, L. Li, J. Alloys Compd. 487 (2009) L5–L7.
[24] P. Stoch, J. Szczerba, J. Lis, D. Madej, Z. Pędzich, J. Eur. Ceram. Soc. 32 (2012) 665–670.
[25] S. Osswald, G. Yushin, V. Mochalin, S.O. Kucheyev, Y. Gogotsi, J. Am. Chem. Soc. 128 (2006) 11635–11642.
[26] A. Achour, A.A. El Mel, N. Bouts, E. Gautron, E. Grigore, B. Angleraud, L. Le Brizoual, P.Y. Tessier, M.A. Djouadi, Diamond Related Mater. 34 (2013) 76–83.
[27] Y. Nosaka, S. Takahashi, Y. Mitani, X. Qiu, M. Miyauchi, Appl. Catal. B: Environ. 111–112 (2012) 636–640.
[28] G.R. Meima, P.G. Menon, Appl. Catal. A: Gen. 212 (2001) 239–245.
[29] O. Shekhah, W. Ranke, R. Schlögl, J. Catal. 225 (2004) 56–68.
[30] X.M. Zhu, M. Schön, U. Bartmann, A.C. van Veen, M. Muhler, Appl. Catal. A: Gen. 266 (2004) 99–108.
[31] W. Weiss, D. Zscherpel, R. Schlögl, Catal. Lett. 52 (1998) 215–220.
[32] Y. Joseph, M. Wühn, A. Niklewski, W. Ranke, W. Weiss, C. Wöll, R. Schlögl, Phys. Chem. Chem. Phys. 2 (2000) 5314–5319.